Available online at www.sciencedirect.com

ScienceDirect

IFAC PapersOnLine 55-38 (2022) 26–32

Control of an Orbital Manipulator with Reaction Wheels for On-orbit Servicing

Ria Vijayan * **Marco De Stefano** * **Christian Ott** **

* *German Aerospace Center (DLR) (e-mail: ria.vijayan@dlr.de, marco.destefano@dlr.de)*
** *TU Wien (e-mail: christian.ott@tuwien.ac.at).*

Abstract: In on-orbit servicing missions, a spacecraft equipped with a manipulator arm grasps a client satellite. Afterwards, the momentum-dumping phase follows and the manipulator can be utilized for servicing tasks. Once the momentum has been dumped, a desired manipulator configuration and base attitude may be needed for initializing a servicing phase such as berthing. The proposed approach prioritizes the attitude maintenance of the servicer spacecraft, and reconfigures the manipulator arm with the grasped client satellite in the nullspace of the servicer's attitude. The approach utilizes the redundancy in rotational degrees of freedom, provided by reaction wheels, to decouple the manipulator reconfiguration task from the attitude of the servicer-base. The proposed controller shows convergence of the attitude and joint-level task, independent of kinematic singularities of the manipulator arm. Additionally, the problem of speed saturation of the reaction wheels is tackled by increasing the damping torques as a function of the wheel speed. Simulation results verify the effectiveness of the proposed control approach.

Keywords: On-orbit Servicing, Orbital Manipulator, Reaction Wheels.

1. INTRODUCTION

On-orbit servicing (OOS) includes tasks such as grasping, berthing and repairing satellites in space using a servicer, which in this paper is considered to be a robotic manipulator arm mounted on top of a base spacecraft equipped with reaction wheels. These so-called orbital manipulators, pose a challenge in the control design due to their floating nature in space. The coordinated control of spacecraft and manipulator can enhance the versatility in operations that can be performed by the servicer for orbital servicing. Recent studies on on-orbit servicing missions (see e.g. the DEOS mission Rank et al. (2011), the COMRADE or the e.Deorbit project Colmenarejo et al. (2018), Telaar et al. (2017)), consider a free-tumbling client satellite i.e. a non-cooperative satellite which no longer has attitude and orbit control capabilities. Therefore stabilizing such a satellite while maintaining the attitude of the servicing spacecraft presents a challenge (Aghili (2009)).

Several works address different strategies to control the motion of the robotic arm and base spacecraft in a coordinated way, while meeting mission requirements and system constraints (see e.g. Dubowsky and Papadopoulos (1993); Moosavian and Papadopoulos (2007)). Giordano et al. (2017) decouples the internal dynamics of the manipulator and reaction wheels from the external center-of-mass motion to do coordinated control. The challenge of actuating the base and manipulator at different frequencies is tackled in De Stefano et al. (2019). Teleoperation and autonomous control are explored as a shared control strategy in Mishra et al. (2021) to achieve base and end-effector control tasks. Multi-arm orbital robot control is developed by Papadopoulos and Moosavian (1994), for the approach and capture phases.

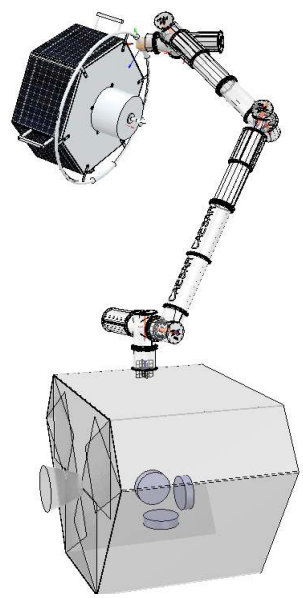

Fig. 1. Bottom: servicer satellite, with 3 mutually orthogonal reaction wheels, and a manipulator arm (CAESAR arm Beyer et al. (2018)). Top: captured client satellite.

The control of orbital manipulators without the use of thrusters on the servicing spacecraft, has reduced flexiblity as compared to coordinated control methods discussed above. In such cases, the conservation of momentum must be taken into account while developing control strategies

10.1016/j.ifacol.2023.01.129

for the resulting free-floating dynamics. Masutani and Miyazaki (1989) designed a resolved rate controller using the the generalized Jacobian resulting from the reduced dynamics of the floating-base system. Oki et al. (2008) uses the generalized Jacobian including reaction wheels and a controller is designed at the kinematic level. Further, a time-optimal manipulator trajectory limiting reaction wheel torques, designed using momentum conservation principle, produces zero reaction torques on the base.

The post-grasp phase in an orbital servicing mission deals with stabilization of the servicer's and client satellite's momentum gained from capturing of the client. Past studies have addressed post-grasp stabilization while minimizing disturbances to the attitude of the base. These were motivated by fuel-saving or power constraints of momentum compensating actuators on the base. In Nenchev and Yoshida (1999), the impact momentum is transferred from the base to the manipulator, while using the reaction null space (Yoshida and Nenchev (1995)) to damp the joint velocities. In Dimitrov and Yoshida (2004), post-grasp decoupling of the base attitude and manipulator dynamics is done using the distributed momentum control concept at a velocity level, and the reaction nullspace concept at a dynamic level. Further approaches for post-grasping stabilization consider an optimal trajectory, which limits the interaction torque (see Aghili (2009)). Oki et al. (2011) presents a time-optimal maneuver for detumbling while constraining contact forces. Lampariello et al. (2018) proposes an energy-optimal approach for the post-grasping phase while using a joint tracking controller. In Vijayan et al. (2022), a detumbling strategy was proposed by exploiting the full actuation capability of the servicer and limiting the contact forces at the manipulator end-effector.

In this paper, we propose a control strategy that stabilizes the attitude of the base while reconfiguring the manipulator arm in the nullspace of the base's attitude, which is required for the berthing phase of an OOS mission. The proposed control considers the case in which the system has zero-momentum, i.e. the momentum has been dumped after the grasp. In contrast to Nenchev and Yoshida (1999); Yoshida and Nenchev (1995); Dimitrov and Yoshida (2004), we propose a passivity-based control instead of a feedback-linearized controller to decouple the base and manipulator in a dynamically consistent way (Khatib (1995)) while using a similar nullspace controller. We consider a closed contact between the servicer's end-effector and the client (as considered in e.g. Gangapersaud et al. (2019)), which implies the velocity-matching constraint between the end-effector and client's grasping point. In addition, a joint-level task is added to reorient the manipulator arm to a configuration desirable for further servicing activities (which may be required, see e.g. Lampariello et al. (2018)). In contrast with Giordano et al. (2017); De Stefano et al. (2015) that also use generalized Jacobians, the main task is on the base and not the end-effector, while in this paper a nullspace task is additionally designed to reconfigure the arm. In contrast with Vijayan et al. (2022), the task of arm-reconfiguration, is performed in the base-attitude nullspace and not end-effector nullspace. Further, reaction wheels actuation is used instead of thrusters to reduce the dependence on non-renewable energy sources.

The contribution of this paper is two-fold. First, a controller is developed in order to maintain the attitude of the servicer base, while the manipulator, with the grasped client satellite, is reconfigured the nullspace of the base attitude. This controller guarantees convergence of the joints to the desired positions and can also operate under kinematic singularities of the arm. These tasks are achieved using the actuation of reaction wheels and joint torques. Second, in order to prevent the reaction wheels from reaching saturation speeds, damping control of the reaction wheels is smoothly increased while still applying the modified torques in the nullspace of the base attitude.

The structure of the paper is as follows. Sec. 2 describes the reduced dynamic model of the system. Sec. 3 introduces the controller design for the proposed strategy. Sec. 4 presents the reaction wheel torque variation. Sec. 5 illustrates the results from a dynamic simulation, and Sec. 6 concludes the work.

2. DYNAMICS MODEL

In this section the dynamics model of the servicer and client satellite is presented for the post-grasping phase. The servicer consists of a base spacecraft with 3 reaction wheels and an n Degree of Freedom (DoF) manipulator arm mounted on top of it. The client is an unactuated satellite that is rigidly grasped by the servicer's end-effector in the post-grasp phase.

2.1 Servicer-Client Dynamics Model

The dynamics is modelled using the velocity constraint imposed by the condition of having a rigid grasp between the servicer end-effector and client. This implies that the velocity at the servicer's end-effector and client's grasping point are equal. This velocity constraint can be used to obtain the combined dynamics of the servicer-client system (Aghili (2009)) using the states of the servicer alone as,

$$\boldsymbol{M}\dot{\boldsymbol{v}}_{\boldsymbol{s}} + \boldsymbol{C}\boldsymbol{v}_{\boldsymbol{s}} = \boldsymbol{T}^T\boldsymbol{\tau}, \tag{1}$$

where, $\boldsymbol{M} = \boldsymbol{M}_{\boldsymbol{s}} + \boldsymbol{J}^T\boldsymbol{J}_{\boldsymbol{c}}^{-T}\boldsymbol{M}_{\boldsymbol{c}}\boldsymbol{J}_{\boldsymbol{c}}^{-1}\boldsymbol{J}$,

$$\boldsymbol{C} = \boldsymbol{C}_{\boldsymbol{s}} + \boldsymbol{J}^T\boldsymbol{J}_{\boldsymbol{c}}^{-T}\boldsymbol{C}_{\boldsymbol{c}}\boldsymbol{J}_{\boldsymbol{c}}^{-1}\boldsymbol{J} + \boldsymbol{J}^T\boldsymbol{J}_{\boldsymbol{c}}^{-T}\boldsymbol{M}_{\boldsymbol{c}}\frac{d}{dt}(\boldsymbol{J}_{\boldsymbol{c}}^{-1}\boldsymbol{J}).$$

Here $\boldsymbol{M}_{\boldsymbol{s}}, \boldsymbol{C}_{\boldsymbol{s}} \in \mathbb{R}^{(6+n+3)\times(6+n+3)}$ and $\boldsymbol{M}_{\boldsymbol{c}}, \boldsymbol{C}_{\boldsymbol{c}} \in \mathbb{R}^{6\times 6}$, are the inertia and Coriolis matrices of the servicer and client dynamics respectively. The servicer's state is given by $\boldsymbol{v}_{\boldsymbol{s}} = \begin{bmatrix}\boldsymbol{v}_{\boldsymbol{b}}^T & \dot{\boldsymbol{q}}_{\boldsymbol{m}}^T & \dot{\boldsymbol{q}}_{\boldsymbol{r}}^T\end{bmatrix}^T \in \mathbb{R}^{6+n+3}$ where $\boldsymbol{v}_{\boldsymbol{b}} \in \mathbb{R}^6$, is the Cartesian velocity (linear and angular) of the base in body frame and $\dot{\boldsymbol{q}}_{\boldsymbol{m}} \in \mathbb{R}^n, \dot{\boldsymbol{q}}_{\boldsymbol{r}} \in \mathbb{R}^3$, are the joint and reaction wheel rates respectively. The actuation on the servicer, $\boldsymbol{\tau} = \begin{bmatrix}\boldsymbol{\tau}_{\boldsymbol{m}}^T & \boldsymbol{\tau}_{\boldsymbol{r}}^T\end{bmatrix}^T \in \mathbb{R}^{n+3}$, includes the torques applied to the manipulator joints $\boldsymbol{\tau}_{\boldsymbol{m}} \in \mathbb{R}^n$, and reaction wheels $\boldsymbol{\tau}_{\boldsymbol{r}} \in \mathbb{R}^3$. The servicer's Jacobian matrix, $\boldsymbol{J} = [\boldsymbol{J}_{\boldsymbol{b}}\ \boldsymbol{J}_{\boldsymbol{m}}\ \boldsymbol{0}] \in \mathbb{R}^{6\times(6+n+3)}$, maps $\boldsymbol{v}_{\boldsymbol{s}}$ to the end-effector Cartesian velocity, $\boldsymbol{J}_{\boldsymbol{b}} \in \mathbb{R}^{6\times 6}, \boldsymbol{J}_{\boldsymbol{m}} \in \mathbb{R}^{6\times(n+3)}$, are the base and manipulator Jacobians respectively. $\boldsymbol{J}_{\boldsymbol{c}} \in \mathbb{R}^{6\times 6}$ is the client's Jacobian matrix mapping Cartesian velocity at its center-of-mass to its grasping point. Lastly, the appropriate selection matrix distributing the torques to the manipulator and reaction wheel dynamics is given by $\boldsymbol{T} = \begin{bmatrix}\boldsymbol{0}_{(n+3)\times 6}\ \boldsymbol{I}_{(n+3)\times(n+3)}\end{bmatrix}$.

2.2 Reduced Servicer-Client Dynamics Model

The servicer-client system considered here operates under the condition where external forces and momentum are zero. As we actuate only the manipulator and reaction wheels, a reduced dynamics model can be derived and exploited for the controller design in Sec. 3. In order to reduce the model, let us define reduced coordinates $\dot{\boldsymbol{q}} = \left[\dot{\boldsymbol{q}}_{\boldsymbol{m}}^T \ \dot{\boldsymbol{q}}_{\boldsymbol{r}}^T\right]^T$ given by the relation,

$$\dot{\boldsymbol{q}} = \boldsymbol{T}\boldsymbol{v}_{\boldsymbol{s}}. \tag{2}$$

This implies that servicer states can be retrieved from the reduced coordinates and the generalized momentum of the system as,

$$\boldsymbol{v}_{\boldsymbol{s}} = \boldsymbol{T}^{M+}\dot{\boldsymbol{q}} + \begin{bmatrix} \boldsymbol{M}_{\boldsymbol{b}}^{-1}\boldsymbol{\xi} \\ \boldsymbol{0}_{(\boldsymbol{n}+\boldsymbol{3})} \end{bmatrix} \tag{3}$$

Here $\boldsymbol{T}^{M+} = \boldsymbol{M}^{-1}\boldsymbol{T}^T(\boldsymbol{T}\boldsymbol{M}^{-1}\boldsymbol{T}^T)^{-1}$ is generalized-inverse of $\boldsymbol{T}$. Further, $\boldsymbol{\xi} = [\boldsymbol{M}_{\boldsymbol{b}} \ \boldsymbol{M}_{\boldsymbol{bm}} \ \boldsymbol{M}_{\boldsymbol{br}}]\,\boldsymbol{v}_{\boldsymbol{s}}$ is the generalized momentum (linear and angular) where,

$$\boldsymbol{M} = \begin{bmatrix} \boldsymbol{M}_{\boldsymbol{b}} & \boldsymbol{M}_{\boldsymbol{bm}} & \boldsymbol{M}_{\boldsymbol{br}} \\ \boldsymbol{M}_{\boldsymbol{bm}}^T & \boldsymbol{M}_{\boldsymbol{m}} & \boldsymbol{0} \\ \boldsymbol{M}_{\boldsymbol{br}}^T & \boldsymbol{0}^T & \boldsymbol{M}_{\boldsymbol{r}} \end{bmatrix}, \ \boldsymbol{T}^{T_{M+}} = \begin{bmatrix} -\boldsymbol{M}_{\boldsymbol{bm}}^T\boldsymbol{M}_{\boldsymbol{b}}^{-1} & \boldsymbol{I} & \boldsymbol{0} \\ -\boldsymbol{M}_{\boldsymbol{br}}^T\boldsymbol{M}_{\boldsymbol{b}}^{-1} & \boldsymbol{0} & \boldsymbol{I} \end{bmatrix}. \tag{4}$$

$\boldsymbol{M}_{\boldsymbol{b}} \in \mathbb{R}^{6\times6}, \boldsymbol{M}_{\boldsymbol{m}} \in \mathbb{R}^{n\times n}, \boldsymbol{M}_{\boldsymbol{r}} \in \mathbb{R}^{3\times3}$ are the base, manipulator and reaction wheel inertia matrices and, $\boldsymbol{M}_{\boldsymbol{bm}} \in \mathbb{R}^{6\times n}, \boldsymbol{M}_{\boldsymbol{br}} \in \mathbb{R}^{6\times3}$ are the base-manipulator and, base-reaction-wheel inertia coupling matrices respectively.

We consider a free-floating system without any external momentum i.e. $\boldsymbol{\xi} = \boldsymbol{0}$. As no external forces act on the base, the zero-momentum is conserved, and the servicer states in (3) are given by $\boldsymbol{v}_{\boldsymbol{s}} = \boldsymbol{T}^{M+}\dot{\boldsymbol{q}}$.

The reduced dynamics of the system in (1) can now be transformed using (2) and (3) and it results as follows,

$$\bar{\boldsymbol{M}}\ddot{\boldsymbol{q}} + \bar{\boldsymbol{c}} = \boldsymbol{\tau}, \tag{5}$$

where,

$$\bar{\boldsymbol{M}} = (\boldsymbol{T}\boldsymbol{M}^{-1}\boldsymbol{T}^T)^{-1} = \boldsymbol{T}^{T_{M+}}\boldsymbol{M}\boldsymbol{T}^{M+},$$
$$\bar{\boldsymbol{c}} = \bar{\boldsymbol{M}}\boldsymbol{T}\boldsymbol{M}^{-1}\boldsymbol{C}\boldsymbol{v}_{\boldsymbol{s}} - \bar{\boldsymbol{M}}\dot{\boldsymbol{T}}\boldsymbol{v}_{\boldsymbol{s}} = \bar{\boldsymbol{C}}\dot{\boldsymbol{q}}.$$

where $\bar{\boldsymbol{C}} = \boldsymbol{T}^{T_{M+}}\boldsymbol{C}\boldsymbol{T}^{M+}$ and $\dot{\boldsymbol{T}} = \boldsymbol{0}$. Observe that the reduced dynamics in (5) are none other than the generalized dynamics for a free-floating system (Umetani and Yoshida (1987)). The model reduction being equivalent to a linear coordinate transformation, it is clear that the passivity property $\dot{\boldsymbol{q}}^T(\dot{\bar{\boldsymbol{M}}} - 2\bar{\boldsymbol{C}})\dot{\boldsymbol{q}} = \boldsymbol{0}$ holds for the reduced model.

3. PROPOSED CONTROLLER DESIGN

In this section we define the base Jacobian in terms of the reduced coordinates and design the controller using the reduced model in (5). The main goal of the controller is to maintain the attitude of the base so as to ensure communications with the ground. In addition, the controller reconfigures the manipulator pose to a nominal configuration suitable for further servicing activities. The torques on the manipulator and reaction wheels are designed in such a way that the arm reconfiguration task is achieved in the nullspace of the base attitude maintenance task.

3.1 Base Jacobian in Reduced Coordinates

In order to address the task of maintaining the base's attitude, we first express the base's angular velocity $\boldsymbol{\omega}_{\boldsymbol{b}} \in \mathbb{R}^3$ in terms of the reduced states of the system. Therefore from (3) and zero-momentum condition we can get,

$$\boldsymbol{\omega}_{\boldsymbol{b}} = -\left[\boldsymbol{0} \ \boldsymbol{I}\right]\boldsymbol{M}_{\boldsymbol{b}}^{-1}\left[\boldsymbol{M}_{\boldsymbol{bm}} \ \boldsymbol{M}_{\boldsymbol{br}}\right]\dot{\boldsymbol{q}} = \bar{\boldsymbol{J}}_{\boldsymbol{\omega}}\dot{\boldsymbol{q}}. \tag{6}$$

where $\bar{\boldsymbol{J}}_{\boldsymbol{\omega}}$ is generalized Jacobian for the base angular velocity, which is expressed as,

$$\bar{\boldsymbol{J}}_{\boldsymbol{\omega}} = -\bar{\boldsymbol{M}}_{\boldsymbol{\omega}}^{-1}\left[\bar{\boldsymbol{M}}_{\boldsymbol{\omega m}} \ \boldsymbol{M}_{\boldsymbol{\omega r}}\right]. \tag{7}$$

The inertia terms $\bar{\boldsymbol{M}}_{\boldsymbol{\omega}} = \boldsymbol{M}_{\boldsymbol{\omega}} - \boldsymbol{M}_{\boldsymbol{v\omega}}^T\boldsymbol{M}_{\boldsymbol{v}}^{-1}\boldsymbol{M}_{\boldsymbol{v\omega}}$ and $\bar{\boldsymbol{M}}_{\boldsymbol{\omega m}} = \boldsymbol{M}_{\boldsymbol{\omega m}} - \boldsymbol{M}_{\boldsymbol{v\omega}}^T\boldsymbol{M}_{\boldsymbol{v}}^{-1}\boldsymbol{M}_{\boldsymbol{vm}}$ are obtained using the following structure of the inertia matrices in (4)

$$\boldsymbol{M}_{\boldsymbol{b}} = \begin{bmatrix} \boldsymbol{M}_{\boldsymbol{v}} & \boldsymbol{M}_{\boldsymbol{v\omega}} \\ \boldsymbol{M}_{\boldsymbol{v\omega}}^T & \boldsymbol{M}_{\boldsymbol{\omega}} \end{bmatrix}, \quad \begin{aligned} \boldsymbol{M}_{\boldsymbol{bm}}^T &= \begin{bmatrix} \boldsymbol{M}_{\boldsymbol{vm}}^T & \boldsymbol{M}_{\boldsymbol{\omega m}}^T \end{bmatrix}, \\ \boldsymbol{M}_{\boldsymbol{br}}^T &= \begin{bmatrix} \boldsymbol{0}^T & \boldsymbol{M}_{\boldsymbol{\omega r}}^T \end{bmatrix}. \end{aligned}$$

Here $\boldsymbol{M}_{\boldsymbol{v}}, \boldsymbol{M}_{\boldsymbol{\omega}} \in \mathbb{R}^{3\times3}$ are the base's translational and rotational inertia matrices and, $\boldsymbol{M}_{\boldsymbol{v\omega}} \in \mathbb{R}^{3\times3}, \boldsymbol{M}_{\boldsymbol{vm}} \in \mathbb{R}^{3\times n}, \boldsymbol{M}_{\boldsymbol{\omega m}} \in \mathbb{R}^{3\times n}, \boldsymbol{M}_{\boldsymbol{\omega r}} \in \mathbb{R}^{3\times3}$ are the inertia coupling matrices between the base's linear to angular motion, base's linear to manipulator motion, base's angular to manipulator motion and, base's angular to reaction wheel motion respectively. Further, $\boldsymbol{M}_{\boldsymbol{\omega r}}$ is assumed to be full rank and therefore invertible i.e. the reaction wheels can control 3 rotational degrees-of-freedom. Hence, the Jacobian in (7) has full row-rank independent of the manipulator's configuration-dependent inertia coupling $\bar{\boldsymbol{M}}_{\boldsymbol{\omega m}}$.

3.2 Controller Design with Augmented Task Coordinates

The main task of the controller is to stabilize the attitude of the base and to reconfigure the arm in the nullspace of the base's attitude. To facilitate the design of such a controller, augmented task coordinates are introduced and defined as follows,

$$\begin{bmatrix} \boldsymbol{\omega}_{\boldsymbol{b}} \\ \boldsymbol{v}_{\boldsymbol{n}} \end{bmatrix} = \boldsymbol{J}_{\boldsymbol{N}}\dot{\boldsymbol{q}}, \quad \boldsymbol{J}_{\boldsymbol{N}} = \begin{bmatrix} \bar{\boldsymbol{J}}_{\boldsymbol{\omega}} \\ \boldsymbol{N}^{T_{M+}} \end{bmatrix}. \tag{8}$$

Here $\boldsymbol{N}^{T_{M+}} = (\boldsymbol{N}\bar{\boldsymbol{M}}\boldsymbol{N}^T)^{-1}\boldsymbol{N}\bar{\boldsymbol{M}} \in \mathbb{R}^{n\times n+3}$ is the transposed generalized-inverse of $\boldsymbol{N} = \left[\boldsymbol{I}_{\boldsymbol{n}\times\boldsymbol{n}} \ -\bar{\boldsymbol{M}}_{\boldsymbol{\omega m}}^T\boldsymbol{M}_{\boldsymbol{\omega r}}^{-T}\right]$. $\boldsymbol{N}$ represents the nullspace basis matrix of $\bar{\boldsymbol{J}}_{\boldsymbol{\omega}}$ and the property $\bar{\boldsymbol{J}}_{\boldsymbol{\omega}}\boldsymbol{N}^T = \boldsymbol{0}$ holds true.

The dynamics obtained from the transformation of (5) to augmented task coordinates in (8) are inertially decoupled and results as follows,

$$\underbrace{\begin{bmatrix} \boldsymbol{\Lambda}_{\boldsymbol{\omega}} & \boldsymbol{0} \\ \boldsymbol{0} & \boldsymbol{\Lambda}_{\boldsymbol{n}} \end{bmatrix}}_{\boldsymbol{\Lambda}} \begin{bmatrix} \dot{\boldsymbol{\omega}}_{\boldsymbol{b}} \\ \dot{\boldsymbol{v}}_{\boldsymbol{n}} \end{bmatrix} + \underbrace{\begin{bmatrix} \boldsymbol{\mu}_{\boldsymbol{\omega\omega}} & \boldsymbol{\mu}_{\boldsymbol{\omega n}} \\ \boldsymbol{\mu}_{\boldsymbol{n\omega}} & \boldsymbol{\mu}_{\boldsymbol{nn}} \end{bmatrix}}_{\boldsymbol{\mu}} \begin{bmatrix} \boldsymbol{\omega}_{\boldsymbol{b}} \\ \boldsymbol{v}_{\boldsymbol{n}} \end{bmatrix} = \underbrace{\begin{bmatrix} \boldsymbol{\tau}_{\boldsymbol{\omega}} \\ \boldsymbol{\tau}_{\boldsymbol{n}} \end{bmatrix}}_{\boldsymbol{\tau}_{\boldsymbol{N}}}, \tag{9}$$

where,

$$\boldsymbol{\Lambda} = \boldsymbol{J}_{\boldsymbol{N}}^{-T}\bar{\boldsymbol{M}}\boldsymbol{J}_{\boldsymbol{N}}^{-1}, \quad \boldsymbol{\mu} = \boldsymbol{J}_{\boldsymbol{N}}^{-T}\bar{\boldsymbol{M}}\frac{d}{dt}(\boldsymbol{J}_{\boldsymbol{N}}^{-1}) + \boldsymbol{J}_{\boldsymbol{N}}^{-T}\bar{\boldsymbol{C}}\boldsymbol{J}_{\boldsymbol{N}}^{-1},$$
$$\boldsymbol{J}_{\boldsymbol{N}}^{-1} = \left[\bar{\boldsymbol{J}}_{\boldsymbol{\omega}}^{\bar{\boldsymbol{M}}+} \ \boldsymbol{N}^T\right], \quad \boldsymbol{\tau}_{\boldsymbol{N}} = \boldsymbol{J}_{\boldsymbol{N}}^{-T}\boldsymbol{\tau}. \tag{10}$$

Here $\bar{\boldsymbol{J}}_{\boldsymbol{\omega}}^{\bar{\boldsymbol{M}}+} = \bar{\boldsymbol{M}}^{-1}\bar{\boldsymbol{J}}_{\boldsymbol{\omega}}^T(\bar{\boldsymbol{J}}_{\boldsymbol{\omega}}\bar{\boldsymbol{M}}^{-1}\bar{\boldsymbol{J}}_{\boldsymbol{\omega}}^T)^{-1}$ is the dynamically consistent generalized-inverse of $\bar{\boldsymbol{J}}_{\boldsymbol{\omega}}$. Now the control torques in augmented task coordinates for the dynamics in (9) are chosen as,

$$\boldsymbol{\tau}_{\boldsymbol{\omega}} = 2\boldsymbol{E}^T\boldsymbol{K}_{\boldsymbol{P\omega}}\boldsymbol{\Delta\epsilon} - \boldsymbol{K}_{\boldsymbol{D\omega}}\boldsymbol{\omega}_{\boldsymbol{b}} + \boldsymbol{\mu}_{\boldsymbol{\omega n}}\boldsymbol{v}_{\boldsymbol{n}}, \tag{11}$$

$$\boldsymbol{\tau}_{\boldsymbol{n}} = \boldsymbol{N}\begin{bmatrix} \boldsymbol{K}_{\boldsymbol{Pm}}\boldsymbol{\Delta q}_{\boldsymbol{m}} \\ \boldsymbol{0} \end{bmatrix} - \boldsymbol{N}\begin{bmatrix} \boldsymbol{K}_{\boldsymbol{Dm}}\dot{\boldsymbol{q}}_{\boldsymbol{m}} \\ \boldsymbol{K}_{\boldsymbol{Dr}}\dot{\boldsymbol{q}}_{\boldsymbol{r}} \end{bmatrix} + \boldsymbol{\mu}_{\boldsymbol{n\omega}}\boldsymbol{\omega}_{\boldsymbol{b}}, \tag{12}$$

where $\boldsymbol{\Delta\epsilon} = \eta\boldsymbol{\epsilon^d} - \eta^d\boldsymbol{\epsilon} - \boldsymbol{\epsilon} \times \boldsymbol{\epsilon^d}$ is the vector part of the base's error quaternion and $(\eta, \boldsymbol{\epsilon})$, $(\eta^d, \boldsymbol{\epsilon^d})$ are the base's measured and desired quaternions respectively. The matrix $\boldsymbol{E} = \Delta\eta\boldsymbol{I} + \boldsymbol{S}(\boldsymbol{\Delta\epsilon})$ where $\Delta\eta = \eta\eta^d + \boldsymbol{\epsilon}^T\boldsymbol{\epsilon^d}$ and $\boldsymbol{S}(\cdot)$ is the skew-symmetric cross-product operator. $\boldsymbol{K_{D\omega}} \in \mathbb{R}^{3\times3}, \boldsymbol{K_{Dm}} \in \mathbb{R}^{n\times n}$ and $\boldsymbol{K_{Dr}} \in \mathbb{R}^{3\times3}$ are positive-definite damping gain matrices of the base attitude, manipulator joints and reaction wheels, respectively. $\boldsymbol{K_{P\omega}} \in \mathbb{R}^{3\times3}$, $\boldsymbol{K_{Pm}} \in \mathbb{R}^{n\times n}$ are the positive-definite stiffness matrices for the base attitude and joints respectively.

Finally, the control torques $\boldsymbol{\tau}$ to be applied to the manipulator and reaction wheels can be obtained by transforming the designed torques in augmented coordinates in (11) and (12) back to the reduced coordinates. Using $\boldsymbol{\tau} = \boldsymbol{J_N^T}\boldsymbol{\tau_N}$ from (10), the input to the dynamics in (1) results in,

$$\boldsymbol{\tau} = \underbrace{\bar{\boldsymbol{J}}_{\boldsymbol{\omega}}^T\boldsymbol{\tau_{PD\omega}}}_{\boldsymbol{\tau_1}} + \underbrace{\boldsymbol{N}^{M+}\boldsymbol{N}\boldsymbol{\tau_P}}_{\boldsymbol{\tau_2}} + \underbrace{\boldsymbol{N}^{M+}\boldsymbol{N}\boldsymbol{\tau_D}}_{\boldsymbol{\tau_3}} + \boldsymbol{\tau_c}, \qquad (13)$$

where,

$$\boldsymbol{\tau_{PD\omega}} = 2\boldsymbol{E}^T\boldsymbol{K_{P\omega}}\boldsymbol{\Delta\epsilon} - \boldsymbol{K_{D\omega}}\boldsymbol{\omega_b},$$
$$\boldsymbol{\tau_P} = \begin{bmatrix}\boldsymbol{K_{Pm}}\boldsymbol{\Delta q_m}\\ \boldsymbol{0}\end{bmatrix}, \qquad \boldsymbol{\tau_D} = -\begin{bmatrix}\boldsymbol{K_{Dm}}\dot{\boldsymbol{q}}_{\boldsymbol{m}}\\ \boldsymbol{K_{Dr}}\dot{\boldsymbol{q}}_{\boldsymbol{r}}\end{bmatrix},$$
$$\boldsymbol{\tau_c} = \bar{\boldsymbol{J}}_{\boldsymbol{\omega}}^T\boldsymbol{\mu_{\omega n}}\boldsymbol{v_n} + \boldsymbol{N}^{M+}\boldsymbol{\mu_{n\omega}}\boldsymbol{\omega_b},$$

and $\boldsymbol{\Delta q_m} = \boldsymbol{q_m^d} - \boldsymbol{q_m}$ is the error between the desired manipulator joint angles $\boldsymbol{q_m^d}$ and the measured angles $\boldsymbol{q_m}$.

The proposed control law in (13) is composed of 4 terms. The feedback term, $\boldsymbol{\tau_1}$, allows to maintain the attitude of the base to a desired value. $\boldsymbol{\tau_2}$ allows to reconfigure the joints in the nullspace of the base attitude, while $\boldsymbol{\tau_3}$ damps the joint velocities in addition to stabilizing the reaction wheels. The term $\boldsymbol{\tau_c}$ compensates for the Coriolis coupling[1] between the base's attitude and the nullspace dynamics. The schematic of the proposed controller is shown in Fig. 2.

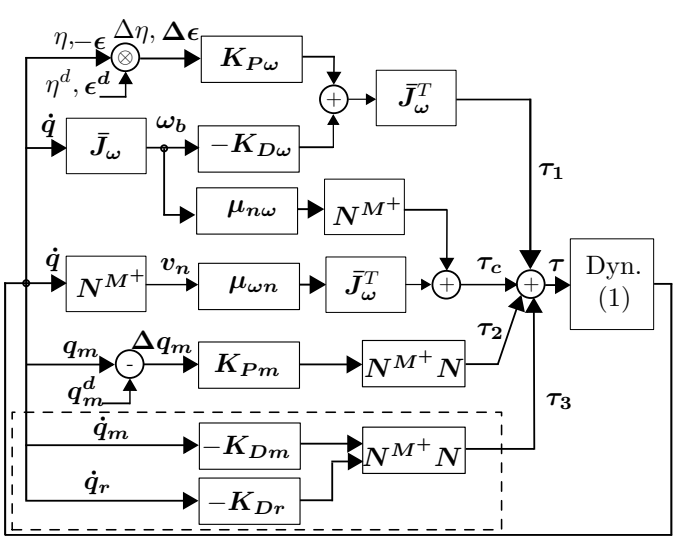

Fig. 2. Block diagram of the proposed controller in closed-loop with the servicer-client dynamics.

[1] Note that $\boldsymbol{\tau_c}$ does not feedback-linearize the complete Coriolis vector, rather only applies the power-conserving Coriolis compensation (Ott et al. (2015)).

It is worth mentioning that, the nullspace $\boldsymbol{N}^{M+}\boldsymbol{N}$ in (13) can be shown to be equivalent to the *angular reaction null space* proposed in Dimitrov and Yoshida (2004), using the relation $\boldsymbol{N}^{M+}\boldsymbol{N} = \boldsymbol{I} - \bar{\boldsymbol{J}}_{\boldsymbol{\omega}}^T\bar{\boldsymbol{J}}_{\boldsymbol{\omega}}^{T\bar{M}+}$. That is, $\boldsymbol{N}^{M+}\boldsymbol{N}$ in (13) projects the inertia coupling $\begin{bmatrix}\bar{\boldsymbol{M}}_{\boldsymbol{\omega m}} & \boldsymbol{M_{\omega r}}\end{bmatrix}$ orthogonal to the metric $\bar{\boldsymbol{M}}^{-1}$. This is a dynamically consistent nullspace projection (Khatib (1995)), which ensures that there is no direct feed-through of angular acceleration to the base due to the nullspace task.

3.3 Convergence of the Controller

The convergence of the controller is analysed in two stages as in Ott (2008). First, conditional stability of the main task shall be shown, and then nullspace stability follows in the set where the main task has converged. Using the theory of semi-definite Lyapunov functions in Iggidr et al. (1996) and Van der Schaft (2000), combined stability of the main task and nullspace task is then argued.

Towards this end, first, the semi-definite Lyapunov function $V_\omega = \frac{1}{2}\boldsymbol{\omega_b^T}\boldsymbol{\Lambda_\omega}\boldsymbol{\omega_b} + 2\boldsymbol{\Delta\epsilon}^T\boldsymbol{K_{P\omega}}\boldsymbol{\Delta\epsilon}$ is chosen for the main task of base attitude control. For the designed control torque $\boldsymbol{\tau_\omega}$ in (11), $\dot{V}_\omega = -\boldsymbol{\omega_b^T}\boldsymbol{K_{D\omega}}\boldsymbol{\omega_b}$ (which follows from the passivity property retained through the coordinate transformations from (1) through (5) to (9)). This shows conditional stability to the set where $\boldsymbol{\omega_b} = \boldsymbol{0}$.

Second, the Lyapunov function $V_n = \frac{1}{2}\boldsymbol{v_n^T}\boldsymbol{\Lambda_n}\boldsymbol{v_n} + \frac{1}{2}\boldsymbol{\Delta q_m^T}\boldsymbol{K_{Pm}}\boldsymbol{\Delta q_m}$ is chosen in the set where $\boldsymbol{\omega_b} = \boldsymbol{0}$ and the designed nullspace control torque $\boldsymbol{\tau_n}$ in (12) leads to $\dot{V}_n = -\boldsymbol{v_n^T}\boldsymbol{N}\begin{bmatrix}\boldsymbol{K_{Dm}} & \boldsymbol{0}\\ \boldsymbol{0} & \boldsymbol{K_{Dr}}\end{bmatrix}\boldsymbol{N}^T\boldsymbol{v_n}$ (which follows similarly to the base task from the passivity property).

Finally, stability is concluded by invoking LaSalle's invariance principle and using the theory of semi-definite Lyapunov functions in Iggidr et al. (1996) and Van der Schaft (2000). This means $\boldsymbol{\omega_b} \to \boldsymbol{0}$ and $\boldsymbol{v_n} \to \boldsymbol{0}$, and $\boldsymbol{\Delta\epsilon}$ converges to an equilibrium where the compliant frame aligns with the desired frame (Caccavale et al. (1999)).

Further, notice that the stiffness term in (12) is responsible for driving the system to, the minimum of the potential $\frac{1}{2}\boldsymbol{\Delta q_m^T}\boldsymbol{K_{Pm}}\boldsymbol{\Delta q_m}$. This minimum occurs when,

$$\underbrace{\begin{bmatrix}\boldsymbol{I_{n\times n}} & -\bar{\boldsymbol{M}}_{\boldsymbol{\omega m}}^T\boldsymbol{M_{\omega r}^{-T}}\end{bmatrix}}_{\boldsymbol{N}}\begin{bmatrix}\boldsymbol{K_{Pm}}\boldsymbol{\Delta q_m}\\ \boldsymbol{0}\end{bmatrix} = \boldsymbol{0}, \qquad (14)$$

i.e when $\boldsymbol{\Delta q_m} = \boldsymbol{0}$, as can be seen from the full rank of the identity matrix that multiplies with the stiffness on the joint errors. Hence, one can also conclude joint task convergence in the nullspace of the base attitude.

The nullspace convergence of the joint task is consistent with the physical understanding that the joints should be able to reorient themselves without disturbing the floating-base's attitude, as long as there are 3 redundant rotational DoFs. The redundant DoFs, provided here by reaction wheels, can hold the attitude of the base by compensating its motion induced by the momentum coupling between the manipulator and base. Notice that this is true independent of the kinematic singularities of the manipulator, evidenced by the term, $\bar{\boldsymbol{M}}_{\boldsymbol{\omega m}}$, not affecting the condition in (14).

4. REACTION WHEEL TORQUE VARIATION

The controller designed in (13) may lead to reaction wheels reaching their saturation speeds. To reduce the demand from the reaction wheels, we investigate which terms can be modified without compromising the primary objectives of the controller.

As introduced in Sec. 3, we see that retaining $\boldsymbol{\tau_1}$ in (13) as designed is necessary for stabilizing and maintaining the attitude of the base for pointing accuracy requirements. It is also desirable to retain $\boldsymbol{\tau_2}$, the stiffness term responsible for the secondary task of reconfiguring the arm. The Coriolis compensation $\boldsymbol{\tau_c}$ is maintained for decoupling the attitude and arm reconfiguration tasks. Therefore damping terms in $\boldsymbol{\tau_3}$ could be modified to alter the rate at which this term drives the system's energy to a stable equilibrium (see Sec. 3.3).

This is done by modifying in particular only the damping on the reaction wheels within the nullspace of the base attitude. Therefore the control torque $\boldsymbol{\tau_3}$ in (13) will consider a new damping gain on the reaction wheels $\boldsymbol{K'_{Dr}}$, and is modified as follows,

$$\boldsymbol{\tau'_3} = -\boldsymbol{N}^{M+}\boldsymbol{N}\begin{bmatrix}\boldsymbol{K_{Dm}}\dot{\boldsymbol{q}}_{\boldsymbol{m}} \\ \boldsymbol{K'_{Dr}}\dot{\boldsymbol{q}}_{\boldsymbol{r}}\end{bmatrix}. \tag{15}$$

where,

$$\boldsymbol{K'_{Dr}} = \boldsymbol{K_{Dr}}\boldsymbol{\sigma}(\dot{\boldsymbol{q}}_{\boldsymbol{r}}). \tag{16}$$

Here $\boldsymbol{\sigma}(\dot{\boldsymbol{q}}_{\boldsymbol{r}}) = \mathrm{diag}(\sigma(\dot{q}_{r_i}))$, is a weighting function that increases the damping on the reaction wheels as they approach their saturation limits as. The weighting function σ chosen here for each *i-th* wheel is, ,

$$\sigma(x) = \begin{cases} x > L_i, & \cosh\left(\frac{|x|-L_i}{U_i-L_i}\mathrm{acosh}(u_i)\right) \\ x \leq L_i, & 1 \end{cases}, \tag{17}$$

where L_i, U_i and u_i are positive constants with $L_i < U_i$. L_i is the lower bound of the wheel speed from where the weighting factor σ starts to increase above 1 along a cosine hyperbolic curve. U_i is the upper bound on the wheel speed where the damping factor increases to a value equal to u_i.

Weighting the damping torques as in (15), preserves the projection into the nullspace of the base attitude. This is essential to avoid the disturbance of the base attitude due to the modified reaction wheel torques. Therefore the controller in (13) is modified with $\boldsymbol{\tau'_3}$ in (15) and the updated schematic is shown in Fig. 3.

The convergence of the modified controller can be shown for the case when the reaction wheel damping gain $\boldsymbol{K_{Dr}}$ in (16) is a diagonal positive-definite matrix. Since the chosen weighting function $\boldsymbol{\sigma}$ will always result in a diagonal and positive-definite matrix, this implies that $\boldsymbol{K'_{Dr}}$ in (16) is also diagonal and positive-definite. Therefore, stability follows from the same arguments made in Sec. 3.3.

5. RESULTS

The simulation is developed in a MATLAB/Simulink framework with an integration time step of 1 ms to validate the proposed control strategy. A servicer spacecraft with three reaction wheels with mass 4 kg and inertia parameters $I_x = 0.0225, I_y = 0.0225, I_z = 0.045, I_{xy} = I_{xz} = I_{yz} = 0$ kgm^2 is considered. The mass and inertia parameters of the servicer base without the reaction wheels is $m = 400$ kg and $I_x = 200, I_y = 250, I_z = 250, I_{xy} = I_{xz} = I_{yz} = 0$ kgm^2. The servicer is also equipped with the 7-DoF DLR CAESAR manipulator arm (see Beyer et al. (2018) for details about the arm). A client satellite with mass $m = 200$ kg and inertia parameters $I_x = 120, I_y = 100, I_z = 90, I_{xy} = -0.5, I_{xz} = -0.8, I_{yz} = -0.4$ kgm^2 is considered. The initial velocity of the servicer considered has a linear base velocity of $[-0.0834\ 0.8963\ -0.3051]^T \times 10^{-3}$m/s, angular base velocity of $[2.9 - 0.4 - 0.4]^T$ deg/s, joint velocities of $[5.4\ 1.2\ -9.6\ 0.4\ 5.5\ 0.3\ -1.3\ ]^T$ deg/s and zero reaction wheel speeds. These states correspond to an initial velocity of the client's center-of-mass of $[5\ 0\ 0]^T$ deg/s and, zero momentum of the combined servicer-client system.

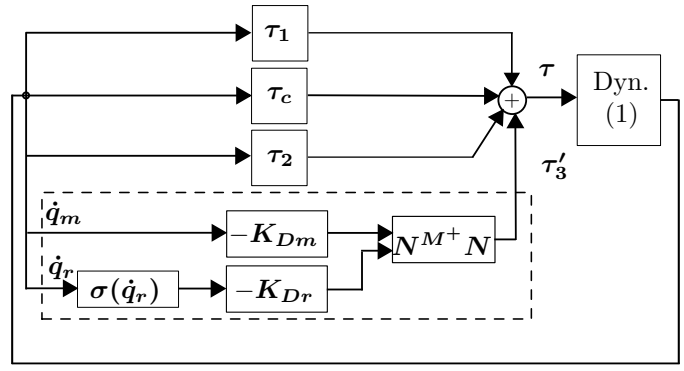

Fig. 3. Block diagram of the modified controller with reaction wheels torque variation. The dashed box shows the difference to the nominal controller design in Fig. 2.

The manipulator arm's initial configuration is chosen as $\boldsymbol{q_m} = [-14\ 22\ 21\ 62\ 140\ -24\ -35]^T$ deg and the desired configuration of the arm at the end of the maneuver is an *elbow-up* configuration, $\boldsymbol{q^d_m} = [0\ 20\ 0\ -45\ 0\ -45\ 0]^T$ deg, suited to ease the berthing task in the subsequent servicing stage. The controller performance is validated for a smooth interpolated trajectory from initial to final joint configuration which approaches a kinematic singularity in between. The controller gains chosen are $\boldsymbol{K_{P\omega}} = 200\boldsymbol{I}_{3\times3}$, $\boldsymbol{K_{D\omega}} = 100\boldsymbol{I}_{3\times3}$, $\boldsymbol{K_{Dq}} = \mathrm{diag}(1,1,1,1,1,5,5) \times 10^2$, $\boldsymbol{K_{Dr}} = 0.01\boldsymbol{I}_{3\times3}$, $\boldsymbol{K_{Pq}} = 4\times10^4\boldsymbol{I}_{7\times7}$. The weighting function parameters in (17) include the wheel speed bounds $L_i = 0.7M_i$ and $M_i = 2000$ rpm, and $m_i = 10$.

The results using the nominal controller (without reaction wheel torque modification) are shown in Fig. 4 and Fig. 5. The manipulator reconfiguration and reaction wheel speeds are shown in Fig. 4 for a simulation time frame of 400 s. The joint errors are seen to converge in Fig. 4 (a), which also shows that the motion of the rigidly grasped client is finally stabilized. The arm is seen to approach a kinematic singularity at approximately 17 in Fig. 4 (c) (where the measure of kinematic singularity approaches a value of zero). Notice, the nullspace task of the manipulator arm reconfiguration is seen to smoothly cross the kinematic singularity. Finally the reaction wheel speeds are shown in Fig. 4 (b). Here we see the wheels spinning in correspondence to the motion of the arm so

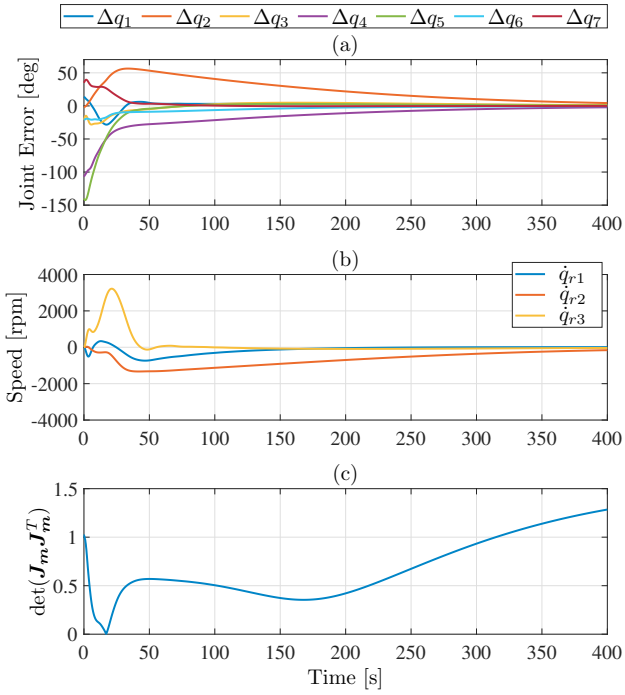

Fig. 4. Manipulator reconfiguration in the nullspace of base attitude using nominal controller in (13). (a) Joint errors (b) Reaction wheel speed (c) Measure of kinematic singularity of the manipulator arm.

as to maintain the attitude of the base. Observe the peak wheel speed of over 3000 rpm.

For better visualization, the base attitude stabilization results using the nominal controller in Fig. 5 are limited to the first 60 s of the simulation. The base attitude is seen to converge in Fig. 5 (a) while the base's angular velocity is damped and stabilized, as seen in Fig. 5 (b). Observe how the arm reconfiguration motion in Fig. 4, which is active beyond the attitude convergence time of approximately 40 s, does not disturb the base's motion in Fig. 5.

[h!] The results for the same scenario simulated with the modified controller that weights the damping on the

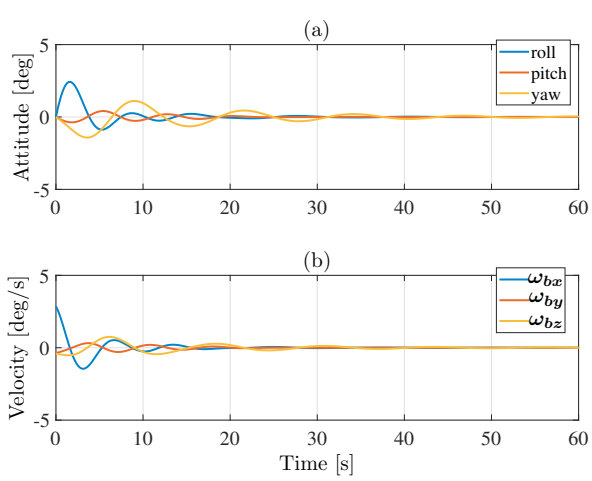

Fig. 5. Base stabilization using nominal controller in (13). (a) Base attitude (b) Base angular velocity.

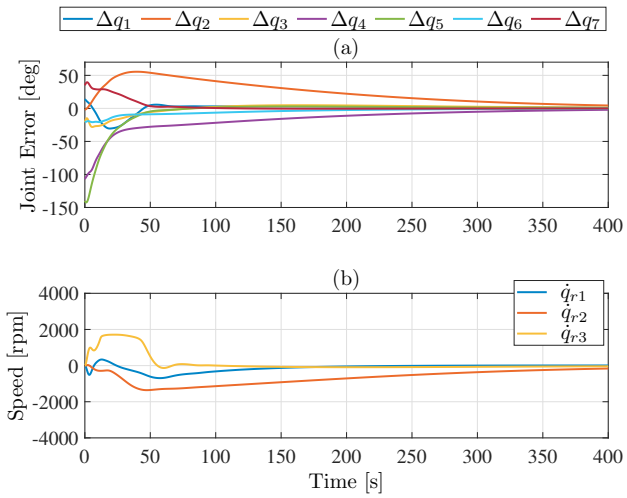

Fig. 6. Manipulator reconfiguration in the nullspace of base attitude using modified controller with reaction wheel torque variation. (a) Joint errors (b) Reaction wheel speed.

reaction wheels is shown in Fig. 6. The evolution of joint errors in Fig. 6 (a) is similar to those in Fig. 4 (a), but upon closer observation, one sees the delay in convergences (see joint 1). The corresponding results of the reaction wheel speed in Fig. 6 (b) show the wheel speeds limited within 2000 rpm. As the results for the base stabilization show no discernible difference in comparison to the results from the nominal controller, the plot for these are omitted. This is however anticipated, since the modifications to the controller are made in the nullspace of the base attitude and therefore the base stabilization motion is expected to be largely unaffected by the minor changes of the system configuration.

These results validate the effectiveness of the designed controller which recongifures the arm without disturbing the attitude of the base while reducing the reaction wheel speeds.

6. CONCLUSION

In this paper, a control strategy for a servicer satellite equipped with reaction wheels has been proposed. The approach exploits the redundancy given by the rotational degrees of freedom of the reaction wheels and allows the reconfiguration of the manipulator in the null space of the attitude of the servicer-base.

The effectiveness of the proposed controller was presented for a post-grasp scenario considering a tumbling servicer-client system with zero-momentum. The performed validation shows that the proposed control can operate also approaching a kinematically singular configuration of the manipulator arm while achieving the reconfiguration of the manipulator. A variation of the damping torques was used to prevent the reaction wheels from reaching speed limits using a weighting function dependent on the wheel speed. The extension of this approach to a servicer with more than three reaction wheels (i.e. having redundant wheels) will be in the scope for future work.

REFERENCES

Aghili, F. (2009). Optimal control of a space manipulator for detumbling of a target satellite. In *IEEE International Conference on Robotics and Automation*, 3019–3024. doi:10.1109/ROBOT.2009.5152235.

Beyer, A., Grunwald, G., Heumos, M., Schedl, M., Bayer, R., Bertleff, W., Brunner, B., Burger, R., Butterfaß, J., Gruber, R., et al. (2018). Caesar: Space robotics technology for assembly, maintenance, and repair. In *Proceedings of the International Astronautical Congress*.

Caccavale, F., Natale, C., Siciliano, B., and Villani, L. (1999). Six-dof impedance control based on angle/axis representations. *IEEE Transactions on Robotics and Automation*, 15(2), 289–300. doi:10.1109/70.760350.

Colmenarejo, P., Branco, J., Santos, N., Serra, P., Telaar, J., Strauch, H., Giordano, A., De Stefano, M., Ott, C., Rainer, M., Henry, D., Jaworski, J., Papadopoulos, E., Visentin, G., Ankersen, F., and Gil-Fernandez, J. (2018). Methods and outcomes of the comrade project - design of robust combined control for robotic spacecraft and manipulator in servicing missions: Comparison between hinf and nonlinear lyapunov-based approaches. In *69th International Astronautical Congress*.

De Stefano, M., Artigas, J., Giordano, A., Lampariello, R., and Albu-Schaeffer, A. (2015). On- ground experimental verification of a torque controlled free-floating robot. In *13th Symposium on Advanced Space Technologies in Robotics and Automation 2015 (ASTRA)*.

De Stefano, M., Mishra, H., Balachandran, R., Lampariello, R., Ott, C., and Secchi, C. (2019). Multi-rate tracking control for a space robot on a controlled satellite: A passivity-based strategy. *IEEE Robotics and Automation Letters*, 4(2), 1319–1326. doi:10.1109/LRA.2019.2895420.

Dimitrov, D. and Yoshida, K. (2004). Momentum distribution in a space manipulator for facilitating the post-impact control. In *IEEE/RSJ International Conference on Intelligent Robots and Systems (IROS)*, volume 4, 3345–3350. doi:10.1109/IROS.2004.1389933.

Dubowsky, S. and Papadopoulos, E. (1993). The kinematics, dynamics, and control of free-flying and free-floating space robotic systems. *IEEE Transactions on Robotics and Automation*, 9(5), 531–543. doi:10.1109/70.258046.

Gangapersaud, R.A., Liu, G., and de Ruiter, A.H.J. (2019). Detumbling a non-cooperative space target with model uncertainties using a space manipulator. *Journal of Guidance, Control, and Dynamics*, 42(4), 910–918. doi:10.2514/1.G003111.

Giordano, A.M., Garofalo, G., and Albu-Schaffer, A. (2017). Momentum dumping for space robots. In *IEEE 56th Annual Conference on Decision and Control (CDC)*, 5243–5248. doi:10.1109/CDC.2017.8264434.

Iggidr, A., Kalitine, B., and Outbib, R. (1996). Semidefinite lyapunov functions stability and stabilization. *Mathematics of Control, Signals and Systems*, 9(2), 95–106.

Khatib, O. (1995). Inertial properties in robotic manipulation: An object-level framework. *The international journal of robotics research*, 14(1), 19–36.

Lampariello, R., Mishra, H., Oumer, N., Schmidt, P., De Stefano, M., and Albu-Schäffer, A. (2018). Tracking control for the grasping of a tumbling satellite with a free-floating robot. *IEEE Robotics and Automation Letters*, 3(4), 3638–3645. doi:10.1109/LRA.2018.2855799.

Masutani, Y. and Miyazaki, F. (1989). Sensory feedback control for space manipulators. *Journal of the Robotics Society of Japan*, 7(6), 647–655.

Mishra, H., Balachandran, R., De Stefano, M., and Ott, C. (2021). A compliant partitioned shared control strategy for an orbital robot. *IEEE Robotics and Automation Letters*, 6(4), 7317–7324. doi:10.1109/LRA.2021.3097509.

Moosavian, S.A.A. and Papadopoulos, E. (2007). Free-flying robots in space: an overview of dynamics modeling, planning and control. *Robotica*, 25(5), 537–547. doi:10.1017/S0263574707003438.

Nenchev, D. and Yoshida, K. (1999). Impact analysis and post-impact motion control issues of a free-floating space robot subject to a force impulse. *IEEE Transactions on Robotics and Automation*, 15(3), 548–557. doi:10.1109/70.768186.

Oki, T., Abiko, S., Nakanishi, H., and Yoshida, K. (2011). Time-optimal detumbling maneuver along an arbitrary arm motion during the capture of a target satellite. In *IEEE/RSJ International Conference on Intelligent Robots and Systems*, 625–630. doi:10.1109/IROS.2011.6095159.

Oki, T., Nakanishi, H., and Yoshida, K. (2008). Time-optimal manipulator control of a free-floating space robot with constraint on reaction torque. In *IEEE/RSJ International Conference on Intelligent Robots and Systems*, 2828–2833. doi:10.1109/IROS.2008.4650835.

Ott, C. (2008). *Cartesian impedance control of redundant and flexible-joint robots*. Springer.

Ott, C., Dietrich, A., and Albu-Schäffer, A. (2015). Prioritized multi-task compliance control of redundant manipulators. *Automatica*, 53, 416–423. doi:10.1016/j.automatica.2015.01.015.

Papadopoulos, E. and Moosavian, S.A.A. (1994). Dynamics and control of multi-arm space robots during chase and capture operations. In *IEEE/RSJ International Conference on Intelligent Robots and Systems*, volume 3, 1554–1561. doi:10.1109/IROS.1994.407648.

Rank, P., Mühlbauer, Q., Naumann, W., and Landzettel, K. (2011). The DEOS automation and robotics payload. In *Symp. on Advanced Space Technologies in Robotics and Automation, ASTRA, the Netherlands*.

Telaar, J., Estable, S., De Stefano, M., Rackl, W., Lampariello, R., Ankersen, F., and Gil Fernandez, J. (2017). Coupled control of chaser platform and robot arm for the e.deorbit mission. *10th Int. ESA conference on Guidance Navigation and Control Systems (GNC)*.

Umetani, Y. and Yoshida, K. (1987). Continuous path control of space manipulators mounted on omv. *Acta Astronautica*, 15(12), 981–986. doi:10.1016/0094-5765(87)90022-1.

Van der Schaft, A. (2000). *L2-gain and passivity techniques in nonlinear control*. Springer.

Vijayan, R., De Stefano, M., and Ott, C. (2022). A detumbling strategy for an orbital manipulator in the post-grasp phase. In *IEEE International Conference on Robotics and Automation*.

Yoshida, K. and Nenchev, D. (1995). Space robot impact analysis and satellite-base impulse minimization using reaction null-space. *IEEE International Conference on Robotics and Automation*, 2, 1271–1277.